Astron. Astrophys. 283, 759–778 (1994)

ASTRONOMY AND ASTROPHYSICS

C IV QSO absorption systems and properties of galactic haloes at high redshift*

P. Petitjean[1,2] **and J. Bergeron**[1]

[1] Institut d'Astrophysique de Paris, 98 bis, Boulevard Arago, F-75014 Paris, France
[2] UA CNRS 173-DAEC, Observatoire de Paris-Meudon, F-92195 Meudon Principal Cedex, France

Received 28 June 1993/Accepted 24 September 1993

Abstract. We have obtained high spectral resolution (FWHM=0.6 or 0.35 Å) observations of six high redshift QSOs, $z_{em} > 2.2$, containing lines from 31 metal-rich absorption line systems amongst which 20 C IV doublets splitted in subcomponents with velocity differences within a system smaller than 400 km s^{-1}. Our survey has been combined with published data at similar resolution and the resulting sample comprises 35 systems, 23 of which are splitted in a total of 87 subcomponents. The mean redshift of the sample is $\langle z \rangle = 2.65$.

The distribution of velocity separations is best fitted by two Gaussian components with dispersions of 109 and 525 km s^{-1} and is very similar to the distribution observed in Mg II systems at redshift z$\sim$ 1. The clustering on the smaller scale could be due to relative motions of clouds within galaxy haloes. The small observed value of the one-dimensional velocity dispersion suggests that most of the systems are associated with potential wells characteristic of dwarf galaxies. The larger scale could reflect clustering of haloes in small groups. There are groups of redshifts spanning up to 1200 km s^{-1}; our sample however is not large enough to investigate the clustering up to such velocity differences.

As observed for Mg II systems there is a strong correlation between the total C IV equivalent width of the systems and the number of components. The correlation between the total equivalent width and the total velocity spread, Δv_{max}, is strong for $\Delta v_{max} < 400$ km s^{-1}. For larger velocity spread the equivalent width tends to be smaller than what would be expected from extrapolation of the correlation at smaller velocity differences. Several examples of such highly multiple systems with comparatively small equivalent width have been observed at $z \sim 1.5$. Although they have not been searched for systematically they may be related to a different class of C IV systems and reveal a particular epoch in galaxy formation.

The distribution of C IV column densities for the observed subcomponents is fitted by a power law $dn/dN(\mathrm{C\,IV}) \propto N^{-\beta}$ with $\beta = 1.64 \pm 0.10$ in the range $13.4 < \log N(\mathrm{C\,IV}) < 14.8$.

We have investigated the possible relation between metal line systems and dark matter haloes in the framework of CDM models. The number of C IV systems per unit redshift is well reproduced for $0.3 < z < 1.5$ if the properties of the associated galaxy gaseous haloes do not change much over this redshift range. At higher redshift C IV systems could be associated with the virialized part of haloes with circular velocity $V_c > 70$ km s^{-1}. The large number of Lyman limit systems (LLS) observed at redshift larger than 3 suggests that part of the Lyα forest becomes optically thick at large redshift.

Key words: cosmology: observations – quasars: absorption lines – galaxies: evolution – galaxies: clustering – galaxies: ISM

1. Introduction

QSO absorption line systems are sensitive tracers of absorbing material at any redshift in the range $0 < z < 5$. They are thus a unique tool for studying the evolution of the gaseous component of the universe. There are several pieces of evidence that the metallic absorption line systems are intimately related to galaxies or their precursors.

At high redshift, $z \sim 2$, damped Lyα systems, with neutral hydrogen column densities $N(\mathrm{H\,I}) > 2\,10^{20}$ cm^{-2}, have been shown to contain as much mass as stars at present epoch. They have thus been interpreted as the progenitors of galactic disks (Wolfe 1988). At intermediate redshift, $z \sim 0.6$, Mg II absorption systems have been shown to be associated with bright galaxies (Bergeron 1986; Bergeron & Boissé 1991; Bergeron et al. 1992; Steidel 1993) with very extended gaseous envelopes of radius weakly correlated to luminosity; $R = 35\,h^{-1}(L/L_*)^{0.2}$ kpc ($h = H_0/100$ km s^{-1} Mpc^{-1}). The high detection rate, together with the observed number of Mg II systems, sug-

Send offprint requests to: P. Petitjean

* Based on observations collected at the European Southern Observatory, La Silla, Chile

gests that a large fraction, if not all, of the field galaxy population with luminosity larger than $0.25L_*$ should have large gaseous envelopes. The lack of absorbing galaxies fainter than M_B=19.4 is in apparent conflict with the large number of faint galaxies found at similar redshifts in faint galaxy counts (Colless et al. 1990). This would indicate that these dwarf galaxies have very small or no gaseous halo although this would be surprising given (i) the indication of increased star formation activity in these faint objects (ii) the weak observed dependence of halo radius on luminosity.

Considering the absence of correlation of both the cross-section per galaxy and the total cross-section with redshift and the shape of the luminosity distribution Steidel (1993) concludes that luminous galaxies were already in place at $z > 0.6$ and that they have undergone only modest luminosity evolution. This conclusion is consistent with the interpretation of the damped Lymanα systems at $z \sim 2$ as progenitors of galactic disks (Wolfe 1988). Both observations are however certainly difficult to reconcile with the expected high rate of merging in a flat universe in the framework of CDM models (Frenk et al. 1988; White & Frenk 1991; Kauffmann & White 1993).

The question of how the galactic disks and haloes form can be addressed in part by studying the clustering of metal absorption line systems on small scales. At the smallest scale the distribution of velocity separations between systems should be closely related to the characteristic circular velocity of the haloes (defined as $V_c = [GM(r)/r]^{1/2}$) and at somewhat larger scale to the clustering of the building blocks of today big galaxies. Sargent et al. (1988) have shown that C IV systems significantly cluster on scale smaller than 600 km s^{-1} but velocity separations smaller than 200 km s^{-1} have not yet been investigated.

In fact the properties of these gaseous clouds are still poorly known since their study needs good quality high spectral resolution observations to reveal their internal structure. At spectral resolution $R > 5000$, they usually split into several components spread over very different velocity ranges. The column densities and Doppler parameters vary from one component to the other implying complex kinematical structure and highly variable physical states (see e.g. Blades 1988). Since lines from ions of very different ionization stages can possibly be observed redshifted in the optical from O I which is tied to H I by charge exchange reactions to N V which probes photons of energy larger than the He II ionization potential (54.4 eV), it is possible to discuss the abundances and ionization processes of the gas (Pettini et al. 1983; Steidel 1990b; Wampler 1991; Lanzetta & Bowen 1993; Wampler et al. 1993; Savaglio et al. 1993).

Petitjean & Bergeron (1990) have shown that the distribution of velocity separations between subcomponents of Mg II systems at redshift $z \sim 1$, is best fitted by two Gaussian components with dispersions of 80 and 390 km s^{-1}. They interpret clustering on the smaller scale as due to relative motions of clouds within one absorber and the one on the larger scale as due to groups of such absorbers. The important observation is that the dispersion of the small velocity separations is smaller by at least a factor of two than what is expected as the one-dimensional velocity dispersion of a halo with circular velocity of about 200 km s^{-1} thought to be associated with a today normal galaxy. The aim of this paper is to make a similar study on C IV systems at larger redshift, $z \sim 2.5$. The observations are described in Sect. 2. Notes on individual systems are given in Sect. 3. Clustering of C IV systems is analysed in Sect. 4 and properties of individual components are discussed in Sect. 5. An attempt to relate metal line systems and CDM haloes is made in Sect. 6.

2. Observations

The observations were carried out at the F/8 Cassegrain focus of the 3.6 m telescope at la Silla, ESO Chile. The spectra were obtained with the ESO echelle spectrograph (CASPEC). A 300 line mm^{-1} cross disperser was combined with a 31.6 line mm^{-1} echelle grating. The detector was a

Table 1. Journal of observations

Object	Emission redshift	Date		Integration time (mn)	Wavelength range (nm)	Resolution FWHM (Å)
		Year	Day			
0207–398	2.805	1986	284	100 + 100	488–595	0.6
0237–233	2.224	1984	236	120	564–670	0.6
		1989	266	180	466–570	0.35
		1989	267	180	466–570	0.35
		1989	268	205	466–570	0.35
0420–388	3.12	1985	285	90	531–643	0.6
		1985	286	120	529–639	0.6
0453–423	2.661	1986	13	90 + 100	464–566	0.6
0528–250	2.765	1986	14	100 + 100	485–596	0.6
2126–158	3.28	1984	235	90 + 90	454–573	0.6
		1985	286	90	558–663	0.6

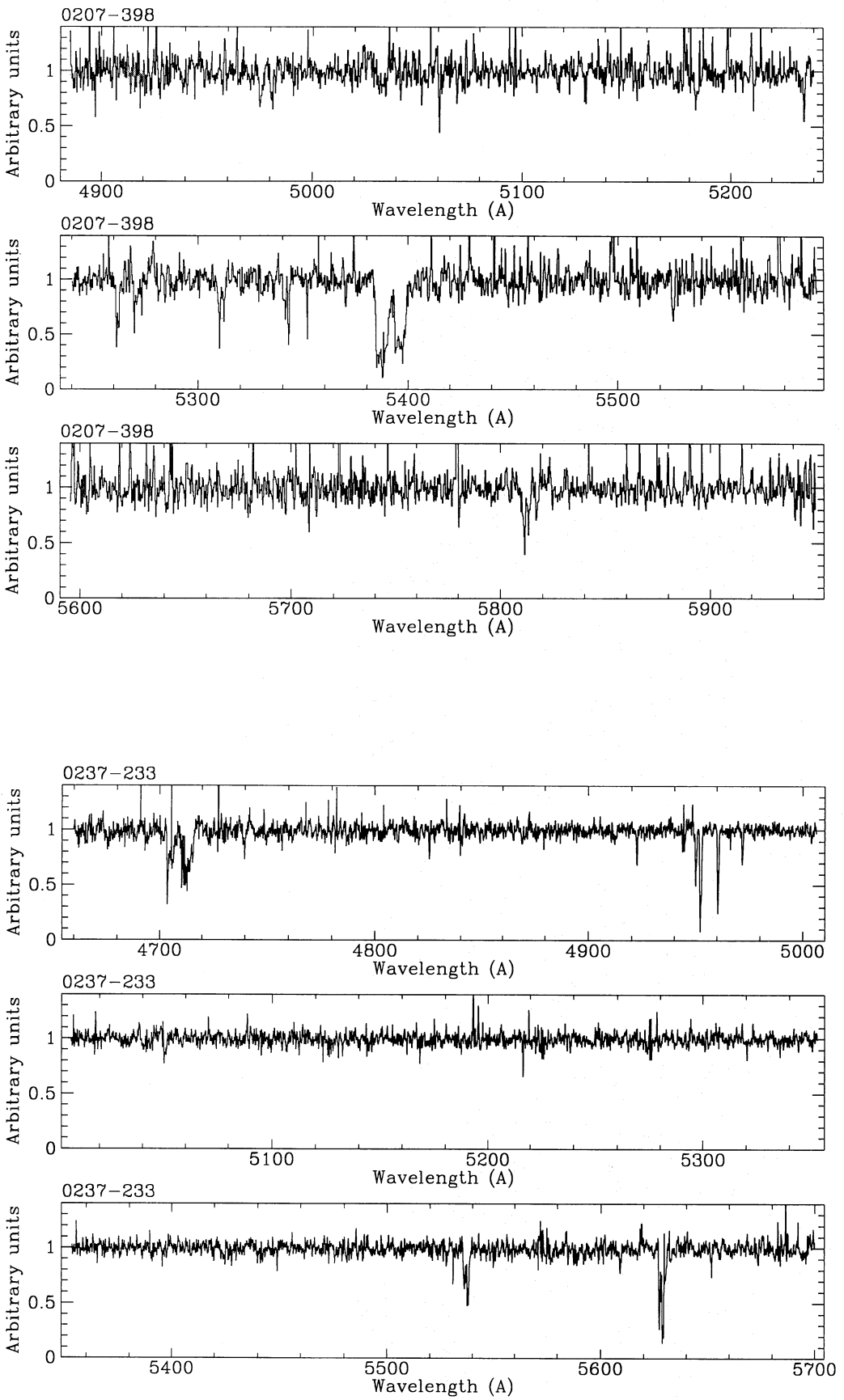

Fig. 1. Normalized spectra of six QSOs

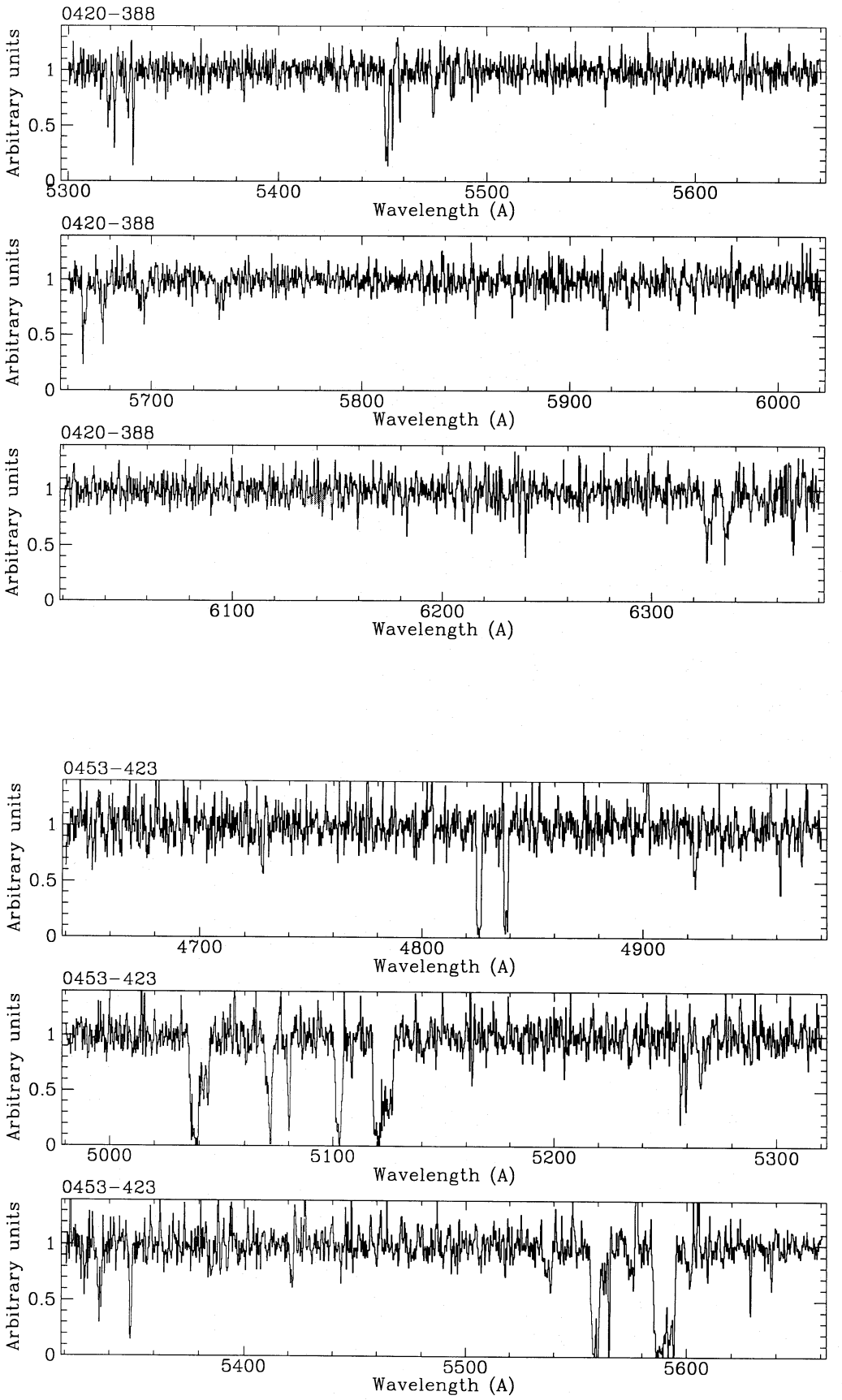

Fig. 1 (continued)

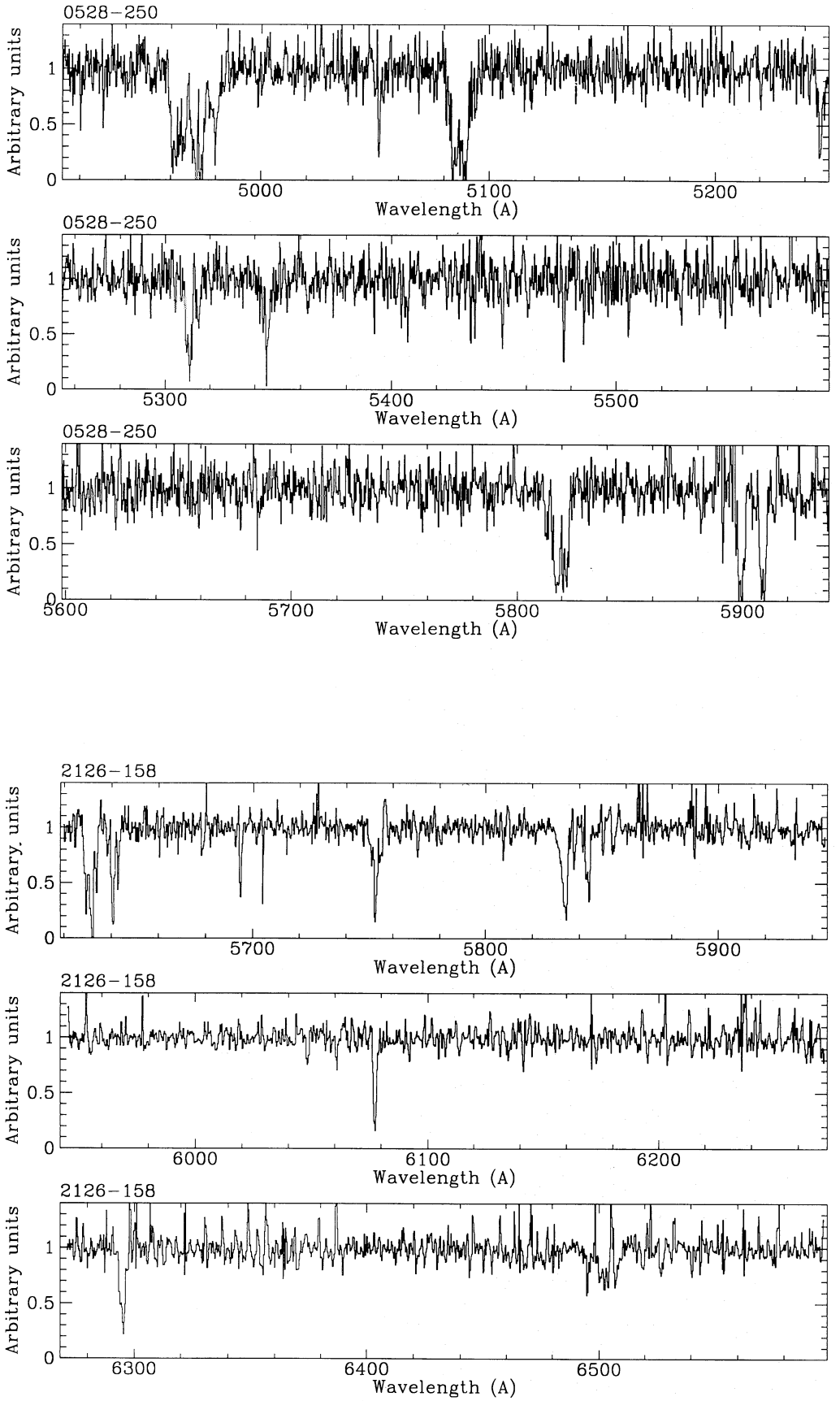

Fig. 1 (continued)

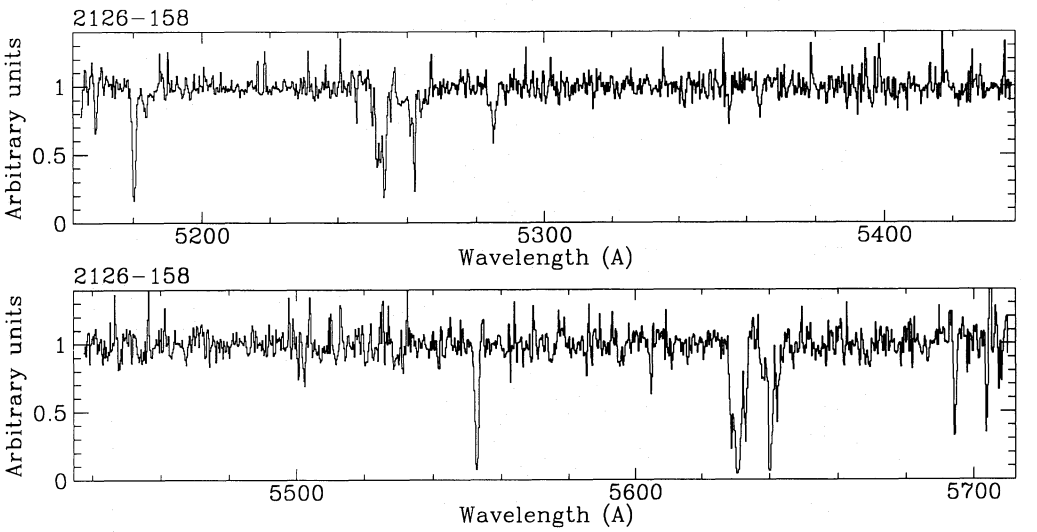

Fig. 1 (continued)

RCA CCD with 320 × 512 pixel of 30 μm square and a read-out noise of 45 electrons rms for all settings but the highest spectral resolution observations of Q0237 − 233 for which a RCA CCD with 640 × 1024 pixel of 15 μm square and a read-out noise of 25 electrons rms was used. The CCD were read-out binned 2 × 2 to decrease the noise relative to the signal. For each exposure on the object flat-field images and wavelength comparison thorium–argon spectra were recorded. The slit width was generally 2″ corresponding to a spectral resolution of FWHM = 0.65 Å or about 2 pixel; for Q0237 − 233 it was 1.5″ giving a resolution FWHM = 0.35 Å. The accuracy in the wavelength calibration measured on the calibrated thorium–argon spectra is about a tenth the resolution quoted above. The data were reduced with the echelle reduction package implemented within MIDAS, the image processing system developed at ESO. The cosmic ray events have been removed in the inter-order using a median filter. The events affecting the object have been identified and removed when combining the orders and the different extracted spectra. This procedure works well when at least three exposures are available. A sky-spectrum is extracted using the pixels adjacent to the object, median filtered and subtracted. The relative small slit length of CASPEC makes this extraction difficult and the accuracy in the sky subtraction is not better than 5%. The journal of observations is shown in Table 1. The results are presented in Fig. 1.

Identified absorption lines are given in Table 2. Wavelengths and redshifts are vacuum and given in the heliocentric rest frame. We have performed profile fittings to all the absorption lines using a synthesis analysis program made available to us by R.F. Carswell (see Carswell et al. 1984; Rauch et al. 1992). The atomic data are taken from Morton et al. (1988) and Morton (1991). The redshifts, velocity dispersions and column densities of subcomponents are given in Table 2.

3. Notes on individual objects

3.1. Q027 − 398 $z_{em} = 2.805$

z_{abs} *=2.2695:* we tentatively identify this weak C IV system with $w_r(\lambda\lambda 154.8, 155.0) = 0.08$ and 0.06 Å respectively (the second line is detected only at the 2σ level).

z_{abs} *=2.3994 and 2.4518:* these two C IV systems are certain and shows two components spanning 56 km s^{-1} and one component respectively.

z_{abs} *=2.4805:* this strong system has been detected by Whelan et al. (1979) and studied by Webb (1987). We observe Si II λ152.6, C IV $\lambda\lambda$154.8, 155.0 and Al II λ167.0. We do not resolve the strong C IV absorption into distinct subcomponents whereas both Al II and Si II absorptions show two subcomponents separated by 110 km s^{-1}. The fit to the C IV doublet alone gives tentatively four components spanning 180 km s^{-1} (see Fig. 2a) two of which correspond to the low ionization subcomponents (see Table 1) adding some confidence in the solution. The column density in each component is poorly defined but the total column density should be of the good order of magnitude.

3.2. Q0237 − 233 z_{em} =2.224

z_{abs} *=1.365:* The Fe II $\lambda\lambda\lambda$234.4, 237.4, 238.2 lines on one hand and the strong Mg II $\lambda\lambda$279.6, 280.3 doublet on the other hand have been independently deblended in four components spanning about 170 km s^{-1} and with redshifts consistent within the error bars (see Table 2 and Fig. 2b). The two ions have column densities of the same order of magnitude as is often the case in Mg II/Fe II systems (Petitjean & Bergeron 1990).

$z_{abs} \sim$ *1.596 and 1.676:* This huge C IV complex has been observed by Boroson et al. (1978), Young et al. (1982) and Sargent et al. (1988). The latter authors count 11 different redshifts with three main subcomplexes at $z_{abs} = 1.596$,

Table 2. Absorption lines

λ_{helio} (Å)	w^a (Å)	σ (Å)	Identification	z_{abs}	n	log N (cm^{-2})	±	b ($km\,s^{-1}$)	±	z_c
0207−398										
5061.85	0.08	0.03	C IV λ1548	2.26951	1	13.7	0.20	10.5	7.	2.26951
5070.26	0.06	0.03	C IV λ1550	2.26951						
5262.95	0.24	0.03	C IV λ1548	2.39940	1	13.7	0.10	13.0	3.	2.39912
					2	13.6	0.10	30.0	7.	2.39976
5271.22	0.14	0.03	C IV λ1550	2.39910						
5312.50	0.26	0.03	Si II λ1526	2.47968	1	13.6	0.05	23.0	3.	2.47905
					2	13.4	0.08	40.0	8.	2.48033
5344.04	0.12	0.03	C IV λ1548	2.45178	1	13.7	0.05	15.0	2.	2.45178
5353.93	0.07	0.03	C IV λ1550	2.45244						
5388.46	1.37	0.14	C IV λ1548	2.48047	1	14.2	0.10	18.0	6.	2.47899
					2	14.9	4.00	4.0	6.	2.47959
					3	13.9	0.40	40.0	24.	2.48061
					4	14.7	0.10	60.0	14.	2.48108
					5	14.8	4.00	4.0	24.	2.48344
5397.44	0.97	0.09	C IV λ1550	2.48049						
5813.68	0.33	0.06	Al II λ1670	2.47956	1	12.7	0.05	36.0	5.	2.47903
					2	12.5	0.08	34.0	8.	2.48025
0237−233										
4718.14	0.28	0.07	C IV λ1548	2.04750						
4719.19	0.38	0.07	C IV λ1550	2.04313						
4928.92	0.06	0.02	Al III λ1854	1.65751	1	12.5	0.19	9.0	9.	1.65750
4950.81	0.08	0.04	Al III λ1862	1.65774						
4956.74	0.15	0.02	Al III λ1854	1.67251	1	13.1	0.10	25.0	5.	1.67249
4958.99	0.28	0.03	C IV λ1548	2.20307	1	14.1	0.08	11.0	2.	2.20287
					2	13.2	0.10	11.0	6.	2.20328
4966.95	0.17	0.02	C IV λ1550	2.20289						
4978.92	0.07	0.02	Al III λ1862	1.67283						
5543.72	0.39	0.04	Fe II λ2344	1.36485	1	13.2	0.60	11.0	16.	1.36442
					2	12.7	1.20	16.0	36.	1.36461
					3	13.7	0.10	39.0	12.	1.36516
					4	12.6	0.60	17.0	29.	1.36573
5615.71	0.05	0.02	Fe II λ2374	1.36505						
5634.64	0.71	0.04	Fe II λ2382	1.36475						
0237−233										
6613.05	1.45	0.13	Mg II λ2796	1.36489	1	12.8	0.08	17.0	5.	1.36419
					2	13.0	0.33	23.0	11.	1.36461
					3	13.6	0.11	38.0	12.	1.36508
					4	12.9	0.30	26.0	8.	1.36556
6630.04	0.95	0.13	Mg II λ2803	1.36489						
0420−388										
5320.65	0.18	0.02	O I λ1302	3.08599	1	14.4	0.15	13.0	9.	3.08579
					2	14.2	1.60	7.0	14.	3.08653
5323.62	0.17	0.02	O I λ1302	3.08827	1	14.7	0.20	14.0	5.	3.08827
5327.62	0.11	0.02	Si II λ1304	3.08444	1	13.4	0.16	14.8	16.	3.08576
					2	13.6	0.11	15.4	10.	3.08648
5332.65	0.13	0.02	Si II λ1304	3.08830	1	15.9	1.70	7.0	4.	3.08837
5452.89	0.37	0.02	C II λ1334	3.08600	1	14.1	0.10	14.4	6.	3.08576
					2	14.9	0.90	15.7	8.	3.08648
5456.05	0.13	0.02	C II λ1334	3.08837	1	14.2	0.50	8.0	4.	3.08837
5475.85	0.19	0.02	C IV λ1548	2.53691						
5485.15	0.08	0.02	C IV λ1550	2.53705						
5669.20	0.26	0.03	C IV λ1548	2.66180	1	13.9	0.03	18.0	3.	2.66152

Table 2 (continued)

λ_{helio} (Å)	w^a (Å)	σ (Å)	Identification	z_{abs}	n	log N (cm^{-2})	±	b ($km\,s^{-1}$)	±	z_c
					2	13.5	0.07	23.0	6.	2.66232
5678.21	0.16	0.03	C IV λ1550	2.66154						
5697.21	0.22	0.02	Si IV λ1393	3.08766	1	13.0	0.11	31.0	13.	3.08625
					2	13.0	0.10	15.0	8.	3.08732
					3	13.2	0.08	36.0	9.	3.08855
5733.75	0.16	0.02	Si IV λ1402	3.08745						
5919.68	0.18	0.03	C IV λ1548	2.82359	1	13.7	0.06	46.0	7.	2.82357
5930.14	0.11	0.03	C IV λ1550	2.82400						
6238.79	0.07	0.03	Si II λ1526	3.08640						
6241.79	0.09	0.02	Si II λ1526	3.08836						
6328.30	0.28	0.04	C IV λ1548	3.08752	1	13.7	0.07	46.0	9.	3.08625
					2	13.8	0.06	31.0	5.	3.08731
					3	13.6	0.08	42.0	10.	3.08854
6337.60	0.26	0.04	C IV λ1550	3.08674						
0453−423										
4826.74	1.32	0.06	Mg II λ2796	0.72608	1	14.2	0.15	54.0	3.	0.72610
4838.98	0.98	0.06	Mg II λ2803	0.72603						
4924.53	0.41	0.06	Mg I λ2852	0.72611	1	12.6	0.07	47.0	9.	0.72610
4962.74	0.10	0.05	Fe II λ2600	0.90861						
5039.45	2.64	0.14	Fe II λ2344	1.14974	1	14.5	0.15	35.0	12.	1.14902
					2	14.4	0.17	58.0	34.	1.14931
					3	14.8	0.52	35.0	15.	1.14975
					4	14.2	0.10	77.0	20.	1.15115
					5	14.3	0.19	14.0	3.	1.15200
5072.90	0.63	0.05	C IV λ1548	2.27664	1	13.4	0.18	12.0	19.	2.27608
					2	14.4	0.04	28.0	3.	2.27668
					3	13.8	0.08	47.0	12.	2.27722
5081.32	0.29	0.05	C IV λ1550	2.27664						
5103.95	1.36	0.07	Fe II λ2374	1.14952						
5109.73	0.13	0.05	Fe II λ2374	1.15196						
5121.82	3.12	0.19	Fe II λ2382	1.14953						
5258.41	0.21	0.03	C IV λ1548	2.39647	1	14.0	0.04	25.0	4.	2.39645
5267.13	0.21	0.03	C IV λ1550	2.39646						
5337.05	0.41	0.05	Mg II λ2796	0.90858	1	13.6	0.05	24.0	3.	0.90855
5350.75	0.47	0.05	Mg II λ2803	0.90858						
5538.84	0.42	0.07	Mn II λ2576	1.14944	1	12.8	0.15	35.0	12.	1.14902
					2	12.8	0.24	58.0	34.	1.14931
					3	13.2	0.12	35.0	15.	1.14974
5560.08	2.11	0.14	Fe II λ2586	1.14954						
5577.00	0.41	0.07	Mn II λ2594	1.14956						
5589.15	3.91	0.14	Fe II λ2600	1.14952						
5602.61	0.28	0.07	Mn II λ2606	1.14952						
5629.66	0.11	0.03	C IV λ1548	2.63626	1	13.8	0.09	10.0	2.	2.63627
5639.06	0.07	0.03	C IV λ1550	2.63630						
0528−250										
4931.32	0.08	0.03	Si IV λ1393	2.53814						
4962.19	1.42	0.08	O I λ1302	2.81070	1	14.2	0.30	21.0	21.	2.80922
					2	14.8	0.20	28.0	15.	2.81030
					3	15.3	0.13	110.0	42.	2.81187
					4	14.5	2.30	4.0	20.	2.81385
					5	14.9	0.20	69.0	21.	2.81452
4971.99	1.39	0.08	Si II λ1304	2.81179	1	13.8	0.22	44.0	24.	2.80839
					2	14.6	0.50	82.0	26.	2.81141
					3	15.0	3.00	18.0	17.	2.81387
					4	13.6	0.24	25.0	21.	2.81472

Table 2 (continued)

λ_{helio} (Å)	w^a (Å)	σ (Å)	Identification	z_{abs}	n	log N (cm^{-2})	±	b ($km\ s^{-1}$)	±	z_c
			C IV λ1548	2.21157	1	14.5	0.13	190.0	56.	2.21162
					2	14.2	0.50	16.0	4.	2.21182
4980.41	0.65	0.03	C IV λ1550	2.21157						
5052.23	0.34	0.03	Fe II λ1608	2.14103	1	13.6	0.22	19.0	20.	2.13996
					2	14.5	0.06	22.6	4.	2.14105
					3	13.7	0.22	39.0	27.	2.14214
5087.21	1.93	0.08	C II λ1334	2.81199	1	14.0	0.30	64.0	30.	2.80839
					2	14.9	0.50	120.0	50.	2.81141
					3	15.4	3.00	28.0	25.	2.81387
					4	14.7	1.50	37.0	22.	2.81472
5221.64	0.07	0.03	Ni II λ1370	2.81086						
5247.75	0.60	0.06	Al II λ1670	2.14084	1	12.3	1.50	5.0	30.	2.13996
					2	13.2	0.04	38.0	5.	2.14087
					3	12.4	0.13	26.0	14.	2.14198
5312.04	0.76	0.07	Si IV λ1393	2.81131	1	13.3	0.50	40.0	20.	2.81001
					2	13.6	0.20	39.0	15.	2.81108
					3	14.1	1.30	1.0	21.	2.81164
					4	13.8	0.60	27.0	18.	2.81218
5346.34	0.47	0.08	Si IV λ1402	2.81128						
5436.30	0.31	0.08	Mg II λ2796	0.94407	1	13.9	2.00	5.0	8.	0.94406
5450.27	0.31	0.08	Mg II λ2803	0.94407						
5477.75	0.18	0.04	C IV λ1548	2.53814	1	14.0	0.11	14.3	4.	2.53813
5486.72	0.10	0.04	C IV λ1550	2.53806						
5819.10	1.63	0.08	Si II λ1526	2.81150						
5900.56	0.88	0.08	C IV λ1548	2.81124	1	13.5	0.30	61.0	24.	2.81001
					2	14.7	0.10	59.0	18.	2.81107
					3	14.9	1.40	1.5	31.	2.81163
					4	13.9	0.30	33.0	12.	2.81218
5911.35	0.75	0.08	C IV λ1550	2.81188						
2126−158										
5181.46	0.33	0.03	Si II λ1526	2.39385	1	12.8	0.40	43.0	55.	2.39318
					2	14.1	0.03	30.0	3.	2.39397
5253.78	0.68	0.03	C IV λ1548	2.39348	1	13.8	0.30	8.0	6.	2.39318
					2	14.2	0.04	21.0	2.	2.39397
			Si IV λ1393	2.76847	1	13.1	0.50	4.0	3.	2.76761
					2	13.4	0.04	23.0	4.	2.76855
					3	12.6	0.42	6.0	15.	2.76937
5263.14	0.27	0.02	C IV λ1550	2.39389						
5286.29	0.15	0.02	Si IV λ1402	2.76847						
5356.19	0.06	0.02	C IV λ1548	2.45962	1	13.3	0.07	24.0	7.	2.45961
5365.16	0.06	0.02	C IV λ1550	2.45968						
5554.02	0.31	0.02	Si II λ1526	2.63787	1	14.2	0.06	25.0	3.	2.63791
5606.04	0.08	0.03	Al III λ1854	2.02259	1	12.9	0.36	6.0	7.	2.02257
5631.92	1.00	0.03	C IV λ1548	2.63772	1	13.9	0.04	29.0	4.	2.63655
					2	14.6	0.03	39.0	2.	2.63783
					3	13.9	0.04	25.0	3.	2.63924
5641.53	0.60	0.03	C IV λ1550	2.63789						
5695.76	0.17	0.03	C IV λ1548	2.67896	1	14.3	0.16	9.0	3.	2.67894
5705.17	0.13	0.03	C IV λ1550	2.67893						
5753.70	0.52	0.03	Si II λ1526	2.76866	1	13.4	0.14	48.0	21.	2.76751
					2	14.2	0.30	15.0	10.	2.76857
					3	13.3	0.42	14.0	23.	2.76906
					4	13.3	0.15	39.0	21.	2.76994
5771.58	0.06	0.02	C IV λ1548	2.72793						
5835.10	0.59	0.03	C IV λ1548	2.76896	1	13.5	0.09	37.0	12.	2.76751

Table 2 (continued)

λ_{helio} (Å)	w^a (Å)	σ (Å)	Identification	z_{abs}	n	log N (cm^{-2})	$\pm$	b (km s^{-1})	$\pm$	z_c
					2	13.8	0.05	22.0	6.	2.76857
					3	14.1	0.09	14.0	3.	2.76906
					4	13.1	0.30	59.0	54.	2.76994
5844.76	0.28	0.03	C IV λ1550	2.76894						
6049.42	0.08	0.02	C IV λ1548	2.90739						
6061.93	0.06	0.02	Fe II λ1608	2.76878						
6296.20	0.48	0.03	Al II λ1670	2.76835	1	12.3	0.50	24.0	21.	2.76751
					2	13.1	0.40	46.0	28.	2.76843
					3	12.2	1.70	21.0	35.	2.76895
					4	11.9	1.30	4.0	19.	2.76962

[a] Rest equivalent width.

1.657 and 1.674. The Mg II and Fe II counterparts have been observed by Boissé & Bergeron (1985) and Lanzetta et al. (1987) at somewhat lower resolution. The w_r(C IV λ154.8)/w_r(Mg II λ279.6) ratio is larger than 3.7, 2.2 and 0.9 in the three subcomplexes respectively. The Al III lines associated with these C IV systems are redshifted in our wavelength range. We detect no Al III line for $z_{abs} = 1.596$ down to an equivalent width of 0.04 Å and only one component for both $z_{abs} = 1.657$ and 1.674 subcomplexes with $w_r = 0.06$ and 0.15 Å respectively. There is a weak feature ($w_{obs} = 0.12$ Å) at λ4832.51 Å which could be associated to Al III λ185.4 at $z_{abs} = 1.6055$ but there is no trace of the second line of the doublet. The w_r(C IV λ154.8)/w_r(Al III λ185.4) ratio is observed to be about 0.5 through the halo of our Galaxy (Sembach & Savage 1992) and is less than 0.03, 0.05 and 0.14 respectively in the three subcomplexes. This suggests that most of the gas in this high redshift complex is mostly highly ionized with some inhomogeneities where Mg II and Fe II are produced. The field around Q0237 − 233 has been searched for other QSOs to provide background sources against which the presence of absorption at the same redshifts could be investigated (Foltz et al. 1993). The latter authors conclude that the complex can be interpreted as a real spatial overdensity of absorbing clouds with a transverse size comparable to its extend along the line of sight. This overall might indicate that some violent event is occuring on a large scale such as the formation of a cluster of galaxies (see also Sect. 5.1). This complex is not unique; an equivalent case can be found in Q0424 − 131 at $z_{abs} = 1.56$ where 11 C IV components are observed spanning 1200 km s^{-1} with only one weak Si II λ152.6 counterpart (Petitjean et al. in preparation). It would be indeed interesting to search for emission lines associated with this kind of complexes.

z_{abs} *=2.045:* this C IV system has been detected by Sargent et al. (1988) who regards it as possible. We find that the two C IV lines of the doublet spread about 230 km s^{-1} with no clear structure. However the corresponding part of the spectrum is very noisy which prevents us from further investigation.

z_{abs} *=2.203:* the unphysical ratio measured in this C IV system by Sargent et al. (1988) was due in their data to C IV λ154.8 being blended with Al III λ185.4 at $z_{abs} = 1.6716$ (see Fig. 1). The system is resolved into two subcomponents spanning 50 km s^{-1}.

3.3. Q0420 − 388 z_{em} =3.12

z_{abs} *=2.5369 and 2.6618:* these are new weak ($w_r = 0.19$ and 0.16Å respectively) C IV systems with associated Lyα lines (Atwood et al. 1985) although the first one is uncertain. The second one has two subcomponents spanning 65 km s^{-1}.

z_{abs} *=2.8237:* This identification is tentative. A feature is detected at the expected wavelength of the redshifted Lyα line but is interpreted by Atwood et al. (1985) as the blend of two strong lines with $z_{abs} = 2.82252$ and 2.82410.

z_{abs} *=3.08599 and 3.08827:* This system shows three fairly well defined subcomponents in O I λ130.2, Si II λ130.4 (Si II λ152.6 is affected by a cosmic ray) and C II λ133.4 spanning 180 km s^{-1} whereas the C IV and Si IV lines look like rather more continuous absorptions. Atwood et al. (1985) give well defined H I column densities for the three subcomponents log N(H I)=19.30, 18.88 and 19.40. Our O I column densities are log N(O I)=14.4, 14.2 and 14.7 giving oxygen abundances of −4.9, −4.7 and − 4.7 which compared to the solar abundance, −3.16, gives depletions of a factor of 55, 35 and 35 respectively.

3.4. Q0453 − 423 z_{em} = 2.661

This QSO has been observed by Carswell et al. (1977) and Sargent et al. (1979) at somewhat lower resolution and by Lanzetta & Bowen (1993) at a resolution of FWHM = 10 km s^{-1} in the wavelength range 401–495 nm.

z_{abs} =*0.7262:* Our derived total column densities and line widths are consistent with the findings of Lanzetta & Bowen (1993).

z_{abs} =*0.9086:* We detect Fe II λ260.0 but not the corresponding Fe II λ258.6 line; Mg II λ279.6 is affected by a cosmic event.

z_{abs} =*1.1497:* We use the four Fe II lines in our wavelength range to constrain a line profile model which contains five subcomponents spanning 415 km s^{-1}. This velocity spread is unusually large compared to what is observed generally in Mg II systems at redshift $z \sim 1$ (Petitjean & Bergeron 1990) and is reminiscent of the 600 km s^{-1} velocity spread in the $z_{abs} = 0.851$ in Q1327 − 206 (Bergeron et al. 1987). The disymmetry in the profile with a strong blend (components 1, 2 and 3 see Table 2 and Fig. 2c) and more diffuse satellites may indicate the presence of two closely related objects. The three associated Mn II lines are detected in the three stronger Fe II subcomponents (see Table 2 and Fig. 2c). The ratio of total column densities N(Fe II)/N(Mn II) $\sim$ 55 is certainly a lower limit since the Fe II lines are much more saturated than the Mn II lines. The Fe/Mn abundance ratio is 120 in the Sun and is smaller in the diffuse interstellar medium due to differential depletion of the two elements onto dust grains, Fe/Mn = 25 and 12.5 in lower and higher column density gas (de Boer et al. 1987). This suggests that the depletion onto dust grains of the two elements is small in this absorption system. A large N(Fe II)/N(Mn II) $\sim$ 68 is also found in the z_{abs} = 0.7262 system towards the same QSO by Lanzetta & Bowen (1993).

z_{abs} = *2.2766:* The fit to this C IV system gives three components spanning 50 km s^{-1} (see Fig. 2c). The associated N V λ123.8 line is strong with w_r = 0.43 Å (Lanzetta & Bowen 1993); no N V λ124.2 line is detected but it could be blended with a Lyα line (Sargent et al. 1979).

z_{abs} =*2.396:* This C IV system shows no structure although in our data the λ155.0 line is wider than the λ154.8 one. There is a feature at λ_{obs} = 5259.36 Å which could be an additional λ154.8 component but with no λ155.0 counterpart.

z_{abs} =*2.6363*: This new weak C IV system, w_r(C IV λ154.8) = 0.11 Å, has a redshift close to the emission redshift and has no N V λ123.8 line associated down to 0.05 Å (Lanzetta & Bowen 1993).

3.5. *PKS0528 − 250* z_{em} =*3.28*

z_{abs} =*0.9441:* We confirm this weak Mg II system detected by Sargent et al. (1988) although the λ279.6 line is affected by noise in our data.

z_{abs} =*2.1408:* Three components spanning 190 km s^{-1} are found in the Al II λ167.0 and Fe II λ160.8 lines associated to this damped Lyα system (Morton et al. 1980). We derive log[N(Fe II)/N(H I)] = −5.8 and log[N(Al II)/N(H I)] = −7.1. These results are consistent with the conclusion by Meyer & York (1987b) and Meyer et al. (1989) that abundances are about a tenth solar and depletion onto dust grains is small.

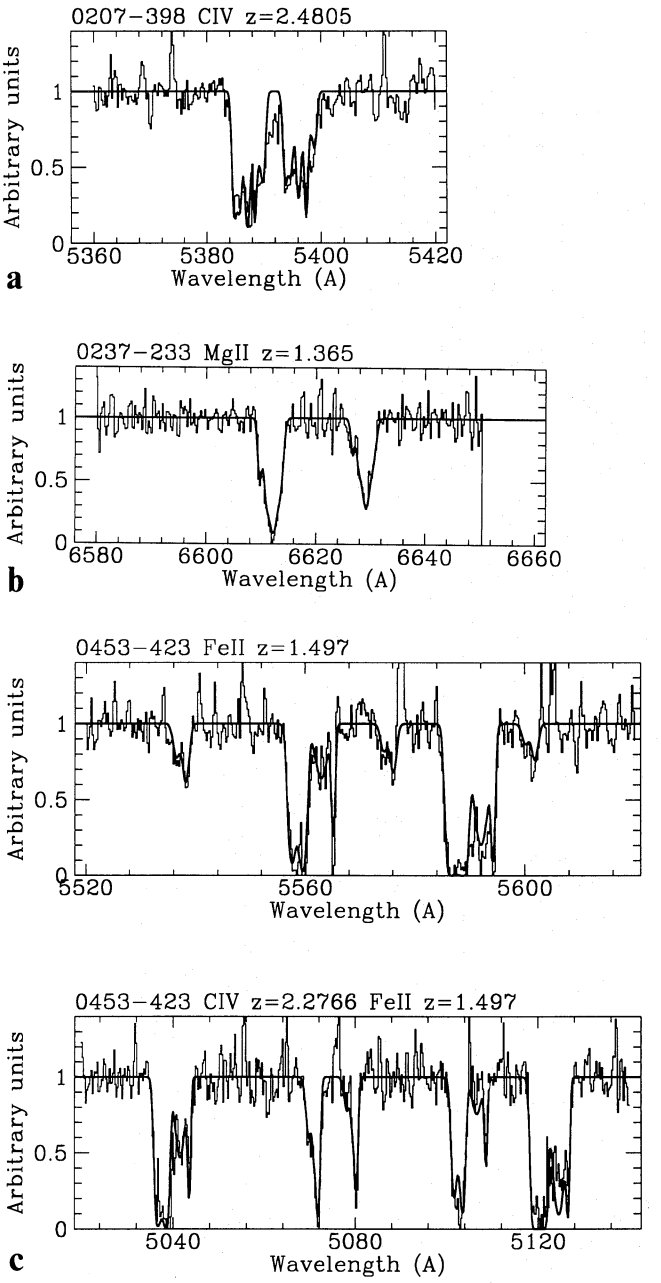

Fig. 2a–c. Model fits for absorption lines. The characteristics of the subcomponents are given in Table 2

z_{abs} =*2.2116:* The λ154.8 line of this strong C IV system is blended with the Si II λ130.4 line at z_{abs} = 2.8107. The general fit of the λ_{obs} = 4972 Å blend and the C IV λ155.0 line gives two components spanning 20 km s^{-1} one of those

with large Doppler parameter value. However the fit of the C IV λ155.0 line is poor.

z_{abs} =*2.5381:* We confirm this single component C IV system with Si IV λ139.3 associated. The Si IV λ140.2 line is blended with O I λ130.2 at $z_{abs} = 2.810$.

z_{abs} =*2.6736:* This system is considered as probable by Sargent et al. (1988). We detect no line with observed equivalent width larger than 0.25 Å.

z_{abs} =*2.8113:* This very strong system is associated with a damped Lyα line (Chen & Morton 1984) in which detection of molecular hydrogen with column density $N(H_2) \sim 10^{18}$ cm^{-2} has been suggested (Levshakov & Varshalovitch 1985; Foltz et al. 1988). Detection of Lyα emission at the same redshift has been claimed by Møller & Warren (1993). A good five component fit spanning 420 km s^{-1} is found for O I λ130.2. One of the components however is rejected when fitting Si II $\lambda\lambda$130.4, 152.6 and C II λ133.4. This is related to the blend of Si II λ130.4 with C IV λ154.8 at $z_{abs} = 2.211$ and to the broad wings of C II λ133.4 (see Fig. 1). In the latter fit the components are spread over 500 km s^{-1}. The Si II total column density we find is consistent within the errors with the value given by Meyer et al. (1989). The H I column density in this system is $1.8\ 10^{21}$ cm^{-2} (Morton et al. 1980) thus most of the neutral hydrogen belongs to a neutral phase where O I is tied to H I by charge exchange reaction (see e.g. Péquignot 1990) and thus the N(O I)/N(H I) ratio is a good indicator of the oxygen abundance. The O I column density is poorly constrained, nevertheless the oxygen abundance is between a tenth and a hundredth solar.

3.6. PKS2126 − 158 z_{em} =3.28

This quasar has been observed recently at higher spectral resolution (FWHM = 14 km s^{-1}), by Giallongo et al. (1993). The derived total column densities compare well with our determinations.

z_{abs} =*2.0226:* This system is mentioned as possible by Sargent et al. (1990) on the basis of strong Lyα line and reasonable C IV lines. We unambiguously detect a single component Al III λ185.4 line. The second line of the doublet is blended with C IV λ154.8 at $z = 2.638$.

z_{abs} =*2.3936:* This system shows two subcomponents spanning 70 km s^{-1} both in Si II λ152.6 and the C IV doublet.

z_{abs} =*2.4596:* We detect no Si II λ152.6 and no Al III lines down to $w_r = 0.03$ Å in this weak C IV system (w_r = 0.06 Å).

z_{abs} =*2.6379:* This system contains a main central subcomponent detected by its Si II λ152.6 and C IV lines plus one satellite line on each side seen only in the C IV lines and spanning 215 km s^{-1} in all.

z_{abs} =*2.6790:* There is only one component at our resolution in this C IV system with no Si II λ152.6 associated ($w_r < 0.03$ Å).

z_{abs} =*2.7279:* We detect the C IV λ154.8 line of this weak system ($w_r = 0.06$ Å) found by Meyer & York (1987a) but not the C IV λ155.0 line which must have an equivalent width very near our detection limit if the system is optically thin.

z_{abs} =*2.7685:* We find four subcomponents spanning 190 km s^{-1} in this system detected by the Si IV and C IV doublets and the Al II λ167.0 and Si II λ152.6 lines. Our column densities are consistent with the determinations by Young et al. (1979).

z_{abs} =*2.9074:* This system has been found by Meyer & York (1987a) and confirmed by Sargent et al. (1990). We detect C IV λ154.8 but not C IV λ155.0.

4. Clustering of C IV clouds

Clustering of C IV systems has been investigated using large samples of absorption systems detected at low resolution (FWHM > 1 Å) (Young et al. 1982; Sargent et al. 1988). The latter authors compute the distribution of the velocity difference between two C IV systems in a sample of systems with $w_r(\lambda 154.8) > 0.15$ Å and with observed velocity separation from the QSO larger than some value βc. When no restriction is applied to βc the distribution shows an excess for $\Delta V < 2000$ km s^{-1}. If the sample is restricted to systems with $\beta c > 5000$ km s^{-1}, the excess remains significant only for $\Delta V < 600$ km s^{-1}. In the absence of further information about what could be the best value for β c to avoid contamination by C IV associated to the QSO it is unclear what part of the signal at smaller velocity separations should be attributed to C IV systems indeed associated with the QSO. Therefore although it is well established that C IV systems do cluster on scale smaller than 600 km s^{-1}, the characteristic clustering scale and the clustering properties at smaller velocity separations have yet to be established.

To address these questions we have increased the sample described in the previous section using data previously published and of similar resolution, namely those of Q0215 + 015 (Pettini et al. 1983), Q1101 − 264 (Carswell et al. 1984), Q2116 − 358 (Wampler et al. 1993) and Q0000 − 2619 (Savaglio et al. 1993). The overall sample is given in Table 3.

Following Sargent et al. (1980) we have estimated the comoving separations between all subcomponents and derived the two-point correlation function for the C IV clouds. Results are presented in Fig. 3 with 60 km s^{-1} bins. The computations have been carried out for $q_0 = 1/2$.

There is adequate information to further investigate the distribution on scales smaller than 1000 km s^{-1}. The normalized distribution for $30 < \Delta v < 1000$ km s^{-1} is shown

Table 3. Characteristics of the subcomopnents

Subcomponent number	z	ΔV (km s^{-1})	C IV		Subcomponent number	z	ΔV (km s^{-1})	C IV	
			log N (cm^{-2})	b (km s^{-1})				log N (cm^{-2})	b (km s^{-1})
0000−2619[a]									
1	3.05410	0.	12.70	7.0	1	4.06880	0.	13.50	30.0
1	3.38810	0.	14.11	20.0	1	4.10100	0.	13.50	20.0
2	3.38890	55.	13.80	15.0	1	4.12600	0.	13.60	13.0
3	3.39010	137.	14.30	20.0	2	4.12700	59.	13.30	20.0
4	3.39090	191.	14.20	20.0	1	4.12970	0.	13.50	12.0
5	3.39150	232.	13.30	8.0	2	4.13100	76.	14.30	18.0
1	3.53580	0.	13.50	20.0	3	4.13230	152.	14.50	18.0
2	3.53700	79.	13.50	20.0	4	4.13340	216.	14.00	12.0
1	4.06060	0.	13.10	20.0	5	4.13420	263.	14.70	23.0
2	4.06170	65.	13.70	40.0					
0207−398									
1	2.26951	0.	13.70	10.0	2	2.47959	52.	14.90	4.0
1	2.39912	0.	13.70	13.0	3	2.48061	140.	13.90	40.0
2	2.39976	56.	13.60	30.0	4	2.48108	180.	14.70	60.0
1	2.45178	0.	13.70	15.0	5	2.48344	383.	14.80	4.0
1	2.47899	0.	14.20	18.0					
0215 + 015[b]									
1	1.49086	0.	13.12	11.0	2	1.64694	323.	13.83	15.0
2	1.49162	92.	13.52	10.0	3	1.64755	392.	13.64	15.0
1	1.54752	0.	14.19	10.0	4	1.64810	455.	13.40	8.0
2	1.54820	80.	13.62	6.0	5	1.64839	487.	13.63	14.0
3	1.54846	111.	13.78	10.0	6	1.64921	580.	14.12	18.0
4	1.55871	140.	13.48	12.0	7	1.64985	653.	13.02	11.0
5	1.54896	170.	14.30	15.0	8	1.65087	768.	13.79	13.5
6	1.54967	253.	13.50	10.0	9	1.65212	910.	13.57	8.0
7	1.55006	299.	13.70	9.0	1	1.68551	0.	13.20	5.0
1	1.64409	0.	13.20	25.0					
0237−233									
1	2.20287	0.	14.10	11.0	2	2.20328	38.	13.20	11.0
0420−388									
1	2.66152	0.	13.90	18.0	1	3.08625	0.	13.70	46.0
2	2.66232	66.	13.50	23.0	2	3.08731	78.	13.80	31.0
1	2.82360	0.	13.70	46.0	3	3.08854	168.	13.60	42.0
0453−423									
1	2.27608	0.	13.40	12.0	1	2.39560	0.	14.00	25.0
2	2.27668	55.	14.40	28.0	1	2.63630	0.	13.80	10.0
3	2.27722	104.	13.80	47.0					
0528−250									
1	2.53814	0.	14.00	14.0	3	2.81163	128.	14.90	2.0
1	2.81001	0.	13.50	61.0	4	2.81218	171.	13.90	33.0
2	2.81107	83.	14.70	59.0					
1101−264[c]									
1	1.83786	0.	13.55	24.0	3	1.83870	89.	13.50	14.0
2	1.83835	52.	13.55	18.0	4	1.83913	134.	13.77	15.0
2116 − 358[d]									
1	1.99494	0.	13.48	30.0	2	2.30625	18.	13.85	8.0
2	1.99555	61.	13.60	8.0	3	2.30658	47.	13.18	8.0
3	1.99594	99.	13.00	20.0	4	2.30680	67.	14.30	5.0
4	1.99621	127.	13.60	10.0	5	2.30709	94.	13.90	8.0

Table 3. (continued)

Subcomponent number	z	ΔV (km s^{-1})	C IV log N (cm^{-2})	C IV b (km s^{-1})	Subcomponent number	z	ΔV (km s^{-1})	C IV log N (cm^{-2})	C IV b (km s^{-1})
5	1.99654	160.	13.90	15.0	1	2.31702	0.	13.65	15.0
6	1.99685	190.	14.18	25.0	2	2.31768	60.	14.08	25.0
7	1.99737	243.	14.30	20.0	3	2.31812	100.	14.00	15.0
1	2.06798	0.	13.07	10.0	4	2.31843	128.	14.70	15.0
2	2.06824	25.	13.26	10.0	5	2.31885	165.	15.00	8.0
1	2.30606	0.	12.70	8.0					
2126−158									
1	2.39318	0.	13.80	8.0	1	2.67896	0.	14.30	9.0
2	2.39397	70.	14.20	21.0	1	2.76751	0.	13.50	12.0
1	2.45962	0.	13.30	24.0	2	2.76857	84.	13.80	6.0
1	2.63655	0.	13.90	29.0	3	2.76906	123.	14.10	3.0
2	2.63783	106.	14.60	39.0	4	2.76994	193.	13.10	54.0
3	2.63924	222.	13.90	25.0					

References: [a] Savaglio et al. (1993). [b] Pettini et al. (1983); [c] Carswell et al. (1984); [d] Wampler et al. (1993).

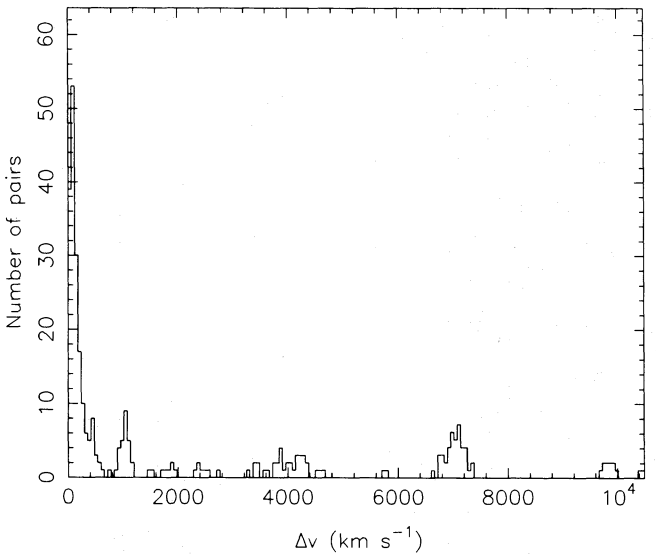

Fig. 3. Two point correlation function for the C IV systems in the sample described in Table 3. The number of line pairs is plotted against the velocity separation Δv in km s^{-1}

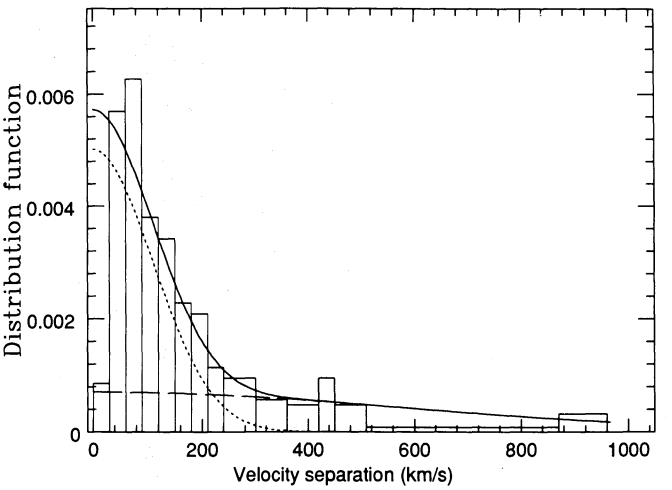

Fig. 4a. Distribution of the velocity separation Δv between two components normalized for Δv in the range 30–1000 km s^{-1}. The sample is described in Table 3. The data are binned with at least 5 points per bin. The solid line is the best fit to the data using a sum of two Gaussian distributions with $\sigma_v = 109$ km s^{-1} (dotted line) and $\sigma_v = 525$ km s^{-1} (dashed line)

in Fig. 4a using bins of different sizes with a minimum width of 30 km s^{-1}, containing each at least 5 pairs. There are 175 pairs in the velocity interval considered. Following Petitjean & Bergeron (1990) we have fitted the distribution using a two-component model of the form

$$f(\Delta v) = \sqrt{\frac{2}{\pi}} \left[\frac{A}{\sigma_a} \exp\left(-\frac{\Delta v^2}{2\sigma_a^2}\right) + \frac{1-A}{\sigma_b} \exp\left(-\frac{\Delta v^2}{2\sigma_b^2}\right) \right]. \quad (1)$$

The best fit and the individual Gaussians are plotted in Fig. 4a. The χ^2 value is 0.24. The probability of this or a greater value is 0.99 for 12 degrees of freedom. The Kolmogorov-Smirnov test on the cumulative distributions gives a maximum difference of 0.04 which has the probability 0.57 to be overtaken. The observed and modeled cumulative distributions are shown in Fig. 5 and it can be seen that the fit is very good up to 450 km s^{-1}, the mod-

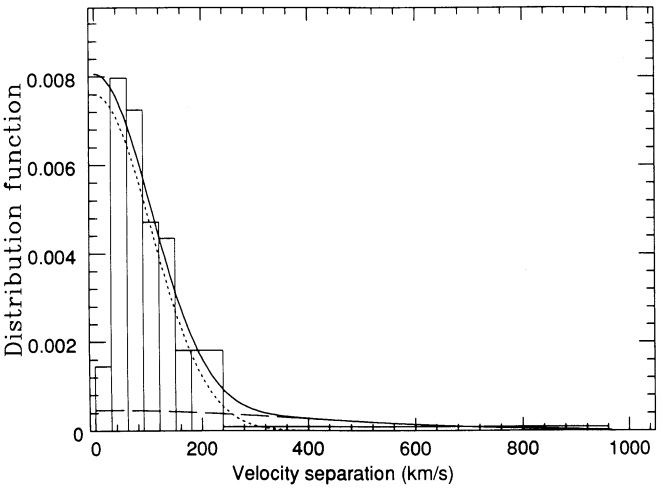

Fig. 4b. Same as Fig. 4a restricting the sample to systems with velocity separation from the QSO larger than 5000 km s^{-1} and excluding the $z_{abs} = 1.649$ system in Q0215 + 015. The solid line is the best fit to the data using a sum of two Gaussian distributions with $\sigma_v = 95$ km s^{-1} (dotted line) and $\sigma_v = 450$ km s^{-1} (dashed line)

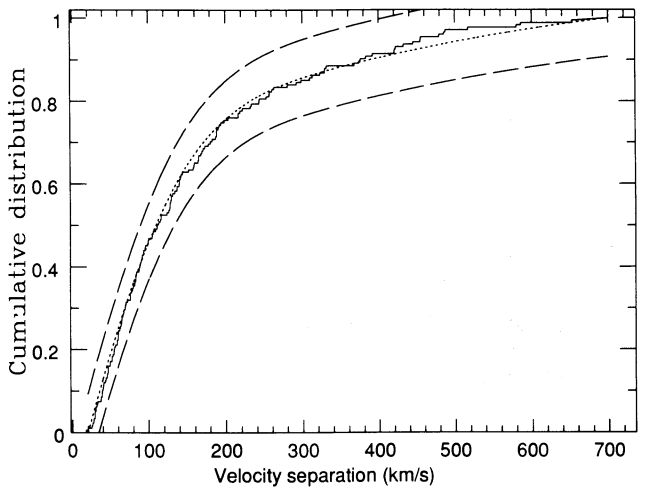

Fig. 5. The observed and fitted cumulative distributions of velocity separations Δv between subcomponents. The fit is the sum of two Gaussian distributions plotted in Fig. 4a. The dashed lines correspond to the 80% confidence level limits for the Kolmogorov–Smirnov test statistics

elled distribution being in excess of the observed one beyond this velocity difference. The fit gives $A = 0.70, \sigma_a = 109$ km s^{-1} and $\sigma_b = 525$ km s^{-1}.

We have carried out the same computation using a subsample containing all C IV systems in Table 3 but with a velocity separation from the QSO larger than 5000 km s^{-1}. It is unclear whether the $z_{abs} = 1.649$ system in Q0215 + 015 has to be removed from the sample since the emission redshift of this BL Lac object is unknown although close to 1.7 (Pettini et al. 1983). In case the system is included in the sample, the best fit to the velocity separation distribution is obtained for $A = 0.63, \sigma_a = 115$ km s^{-1} and $\sigma_b = 470$ km s^{-1}. In case the system is removed from the sample (see also Sect. 5.1), the best fit is for $\sigma_a = 95$ km s^{-1}, $A = 0.9$ and $\sigma_b = 450$ km s^{-1}, the two latter values being poorly constrained. The corresponding distribution function is given in Fig. 4b.

The width σ_a of the Gaussian describing the small velocity differences is well constrained and is in the range 90–120 km s^{-1}. Although it is clear that there exists an excess of velocity separations larger than 300 km s^{-1} as compared to a single Gaussian fit, the width of the broader component is not well defined and could be smaller. It is therefore interesting to note that the distribution is similar to that derived from Mg II systems at $z \sim 1$ by Petitjean & Bergeron (1990) who obtained $\sigma_a = 80$ km s^{-1} and $\sigma_b = 390$ km s^{-1}. Their conclusions thus appear to apply also to C IV systems at $z \sim 2.5$. Most of the subcomponents have velocity separations smaller than 150 km s^{-1} and the velocity separation distribution reflects relative motions of clouds within one halo. The large velocity separations could correspond to the clustering of several haloes.

The similarity between Mg II systems at redshift $z \sim 1$ and C IV systems at $z \sim 2.5$ may gain some support from the detection of candidate galaxies giving rise to C IV systems at $z \sim 1.5$ (Aragón-Salamanca et al. 1993) which are observed to have impact parameters and luminosities comparable to that of Mg II galaxies. However definite answer must await spectroscopic follow-up (see also next section).

5. Physical properties

5.1. Number of components

It has long been recognized that the equivalent width of metal absorption line systems is correlated to the number of components (Wolfe 1986; York et al. 1986; Petitjean & Bergeron 1990). The total rest equivalent width w_r of the C IV systems given in Table 3 is plotted against the number of components n_s in Fig. 6. The dashed line is the best linear fit (the correlation factor is 0.84) for all the points but the one with $n_s = 9$ corresponding to the $z_{abs} = 1.649$ system in Q0215 + 015. The latter system has a small equivalent width compare to the simple linear extrapolation of other values. The number of components is however spectral resolution dependent. We have therefore plotted in Fig. 7 the total equivalent width versus the maximum velocity separation which does not share this disadvantage. The dashed line is the best linear fit and the correlation factor without the above mentioned point is 0.74. It can be seen that the point corresponding to the above mentioned system is well below the fit. Other examples of such system are the $z_{abs} = 1.56$ system in Q0424 − 131 (Sargent et al. 1988) with $w_r = 1.39$ Å and $\Delta v_{max} = 1200$ km s^{-1} (Petitjean et al. in preparation); the $z_{abs} = 1.655$ system

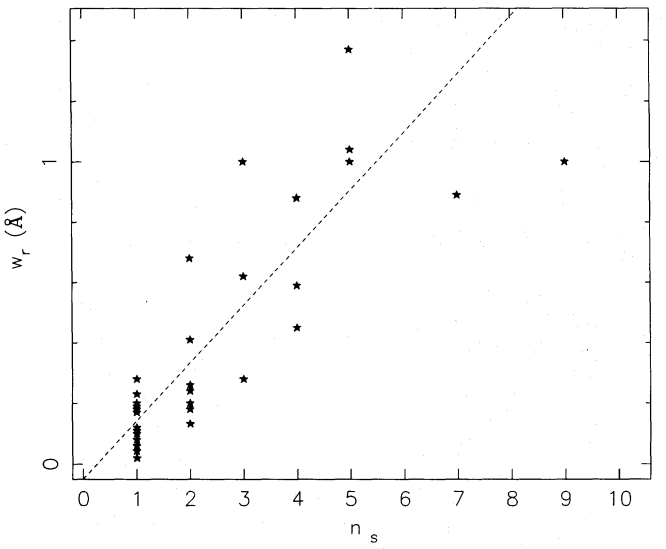

Fig. 6. The total equivalent width (w_r) of C IV λ154.8 versus the number of components (n_s). The dashed line is the linear correlation best fit for all the points but the one with $n_s = 9$

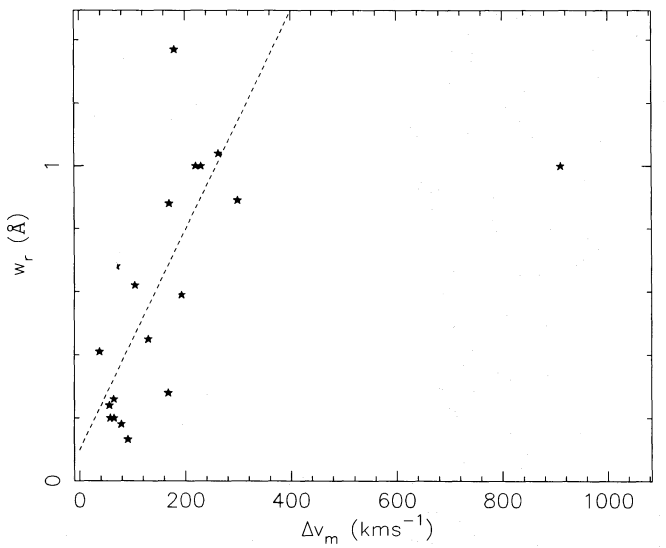

Fig. 7. The total equivalent width (w_r) of C IV λ154.8 versus the maximum velocity separation (v_{max}). The dashed line is the linear correlation best fit for all the points but the one with $v_{max} = 900\ km\ s^{-1}$

in Q0151 + 048 with $w_r \sim 1$ Å and $\Delta v_{max} \sim 750\ km\ s^{-1}$ (Sargent et al. 1988) and the $z_{abs} = 1.658 - 1.673$ system in Q0237 − 233 with $w_r \sim 2.6$ Å and $\Delta v_{max} \sim 2000\ km\ s^{-1}$ (Sargent et al. 1988). These systems could represent the few galaxies or groups of galaxies collapsing in potential wells of large circular velocities (see also Sect. 6). Definite conclusion however must await further detailed spectroscopic studies of the systems and their possible associated galaxies.

5.2. Column density and Doppler parameter

The Doppler parameter b distribution for all subcomponents is given in Fig. 8. As the mean spectral resolution of the present data is about FWHM = 23 km s^{-1} the two first bins are incomplete. The distribution spreads out to large b values. Although some of the lines are most certainly blends of components which will be separated only by higher spectral resolution observations, others are clearly isolated and have b values in excess of 20 km s^{-1} (see Table 3). The origin of the broadening cannot be only thermal since it corresponds to temperatures larger than $3\ 10^5$ K at which carbon is mostly in the C^{+3} form (Arnaud & Rothenflung 1985). If such large b values were confirmed this would imply that the individual clouds should have turbulent or internal large scale motions as suggested by Petitjean et al. (1992).

The equivalent width estimated from the b and N(C IV) values derived for each subcomponent by profile fitting is given versus the column density in Fig. 9. It can be seen that most of the lines are on the linear part of the curve of growth at least for N(C IV)$< 10^{13.7}$ cm^{-2} that is for 61 subcomponents out of 87.

The column density distribution is given in Fig. 10. The data have been fitted, using a maximum likelihood method by a power law function, $dn/dN(\text{C IV}) \propto N(\text{C IV})^{-\beta}$, in the range $3\ 10^{13}$–$6\ 10^{14}$ cm^{-2}. The best fit is obtained for $\beta = 1.64^{-0.08}_{+0.13}$. There is a turn over of the distribution for smaller column density which may be due to the overall detection limit of the sample. It is intriguing that the index corresponds to that found for the Lyα cloud H I column density distribution derived from high resolution data (Carswell et al. 1991). Eventhough the N(H I) distribution function show several departures from a single power law the latter is a good approximation for $10^{14} < N(\text{H I}) < 10^{16}$ cm^{-2} (Petitjean et al. 1993). The H I column den-

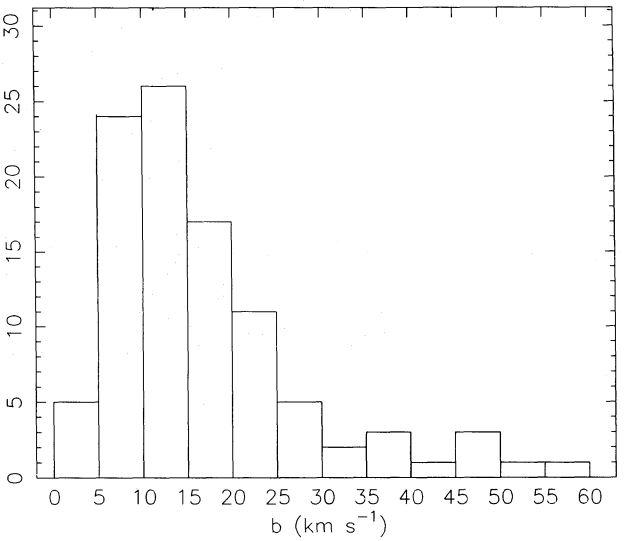

Fig. 8. Histogram of the distribution of intrinsic velocity dispersion for the subcomponents given in Table 3

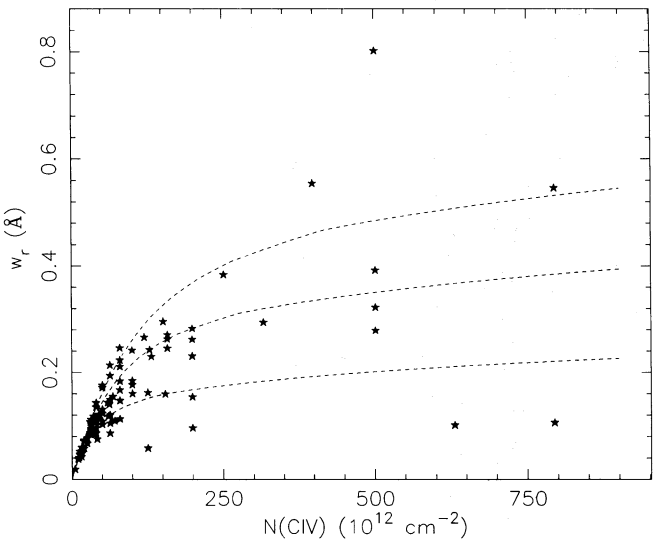

Fig. 9. Rest equivalent width of C IV λ154.8 of each component given in Table 3 as a function of the column density (in units of 10^{12} cm^{-2}). Curves of growth are plotted for velocity dispersions b of 10, 20, 30 km s^{-1} (from bottom to top)

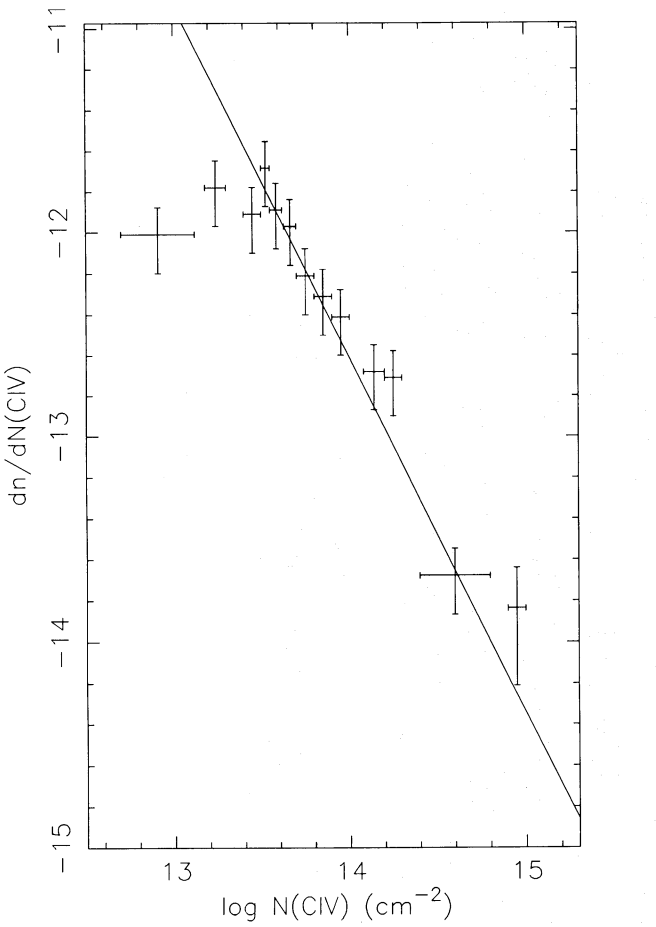

Fig. 10. Logarithm of the C IV column density distribution as a function of the logarithm of the C IV column density. The best single power-law fit obtained by the maximum likelihood method, $dn/dN(\mathrm{C\,IV}) \propto N^{-\beta}$ with $\beta = 1.64$ is also shown. The data have been averaged into bins only for their presentation

sity associated with one C IV component can be written as

$$N(\mathrm{H\,I}) = 8.8 N(\mathrm{C\,IV}) \left(\frac{\mathrm{H\,I/H}}{10^{-4}}\right) \left(\frac{\mathrm{C\,IV/C}}{0.4}\right)^{-1} \times \left(\frac{Z(\mathrm{C})}{0.03 Z_\odot}\right)^{-1}, \quad (2)$$

with the carbon solar abundance $Z_\odot(\mathrm{C}) = 4.7\,10^{-4}$. The values $\mathrm{C}^{+3}/\mathrm{C} = 0.4$, H I/H $= 10^{-4}$, $Z(\mathrm{C}) = Z_\odot/30$ apply to a C IV absorbing region of average properties as given by photoionization models of metallic absorption line systems (Petitjean et al. 1992).

For $13 < \log N(\mathrm{C\,IV}) < 14.5$ and the above parameters the H I column density would be in the range $14 < \log N(\mathrm{H\,I}) < 15.5$. Larger H I column densities are expected for lower C abundances and lower $\mathrm{C}^{+3}/\mathrm{C}$ ionic ratio. The latter condition is satisfied only if the ionizing spectrum contains a non negligible amount of photons with energy larger than 54.4 eV. This suggests that some Lyα forest systems with H I column densities in the range $14 < \log N(\mathrm{H\,I}) < 16$ should in fact have associated C IV absorptions with $0.05 < w_r < 0.15$ Å (see Fig. 9) as already mentioned by Meyer & York (1987a). As the Lyα systems with H I column densities in the above range are known to show no clustering on scale larger than 50 km s^{-1} (Webb 1987), the large proportion in our sample of C IV systems with a single component, 14 out of 37, strengthens the conclusion.

6. C IV systems and CDM haloes

At intermediate redshift, $z \sim 0.6$, Mg II absorption systems have been shown to be associated with bright galaxies (Bergeron & Boissé 1991; Steidel 1993 and references therein). The galactic halo radius depends weakly upon the galaxy luminosity, $R \propto L^{0.2}$, and there is no significant evolution of R with z over the small redshift range $0.3 < z < 0.7$.

Little is known about the nature of C IV absorbers. Identification of the objects causing low redshift C IV systems (without associated Mg II absorption) detected by the HST (Bahcall et al. 1993) will bring new clue on the C IV absorber population at $z < 1$. At higher redshift, detection of C IV absorbers may prove difficult due to their expected faint magnitude. Up to now, only a tentative detection of L_* galaxies producing highly multiple and strong C IV systems at $z > 1.5$ has been reported (Aragón-Salamanca et al. 1993). This study suggests that C IV absorption-selected galaxies have luminosities and impact parameters comparable to those of the lower redshift Mg II absorbers.

In the framework of CDM models, dark matter haloes of increasing circular velocities collapse due to gravity. The density of the gas falling into these potential wells increases and cooling becomes efficient enough to induce star formation (White & Rees 1978; White & Frenk 1991). Galaxies

then could build up by merging of lower mass haloes although the relation between merging of dark matter haloes and their stellar component is not well established (Frenk et al. 1988; Carlberg & Couchman 1989).

The gas giving rise to C IV systems has been enriched in heavy elements and thus at high redshift must be associated in some way with star formation sites and therefore with haloes of large enough circular velocities. To investigate this relation we have computed the number of absorption systems per unit redshift expected under simple assumptions (see also Mo et al. 1993). We use the Press–Schechter statistics (Press & Schechter 1974) applied to CDM haloes of circular velocity V_c and mass M given by

$$M = \frac{4\pi}{3}\rho_0 r_0^3, \quad V_c = 1.67(1+z)^{1/2} H_0 r_0 \,, \tag{3}$$

where ρ_0 is the mean density of the universe and r_0 the comoving radius of the halo. The comoving number density of haloes per Mpc^3 and unit velocity (in km s^{-1}) is

$$n(V_c, z)\,\mathrm{d}V_c = \frac{-3(1.67)^3\delta_c H_0 (1+z)^{5/2}}{(2\pi)^{3/2} V_c^4 \Delta(r_0)} \frac{\mathrm{d}\ln\Delta}{\mathrm{d}\ln V_c} \times \exp\left(\frac{-\delta_c^2(1+z)^2}{2\Delta^2(r_0)}\right) \mathrm{d}V_c \,, \tag{4}$$

where

$$\Delta(r_0) = 16.3 b_i^{-1}(1 - 0.3909 r_0^{0.1} + 0.4814 r_0^{0.2})^{-10} \,, \tag{5}$$

and b_i is the bias parameter; $\Delta(16\ \mathrm{Mpc}) = 1$ for $b_i = 1$ (see White & Frenk 1991 for a complete discussion).

The number of systems per unit redshift observed on a line of sight is (see Sargent et al. 1980),

$$\frac{\mathrm{d}N(z)}{\mathrm{d}z} = \frac{c}{H_0}(1+z)^{0.5} \int_{V_1}^{V_2} n\pi R^2 \,\mathrm{d}V_c \,, \tag{6}$$

where R is the radius of the absorption system associated with the halo of circular velocity V_c. Some assumption on R has to be made. At low redshift we assume that C IV haloes have the same characteristics as Mg II ones. Thus for $z < z_i$ the radius is defined as

$$R_{\mathrm{lr}} = R_{\mathrm{lr,o}} h^{-1} \left[\frac{M(V_c)}{M(220\ \mathrm{km\,s^{-1}})}\right]^{0.2} , \tag{7}$$

independent of redshift, where we assume that mass is proportional to luminosity. At larger redshift, the radius is assumed to be a fraction f of that of the virialized region

$$R_{\mathrm{hr}} = 0.1 H_0^{-1}(1+z)^{-3/2} V_c f \,. \tag{8}$$

The integration is carried out between V_1 and $V_2 = 400$ km s^{-1}. The latter velocity is taken to correspond to a large galaxy but the exact value has little effect on the results. We also assume that no halo with velocity smaller than V_1 can give rise to a C IV system. The value of V_1 is a free parameter at large redshift. At small redshift, we choose $V_1 = 100$ km s^{-1} since (i) this corresponds to the circular velocity of a $L \sim 0.2 L_*$ galaxy, assuming that the M/L ratio is independent of M and L and that a galaxy of luminosity L_* is associated with a halo of circular 220 km s^{-1}, and (ii) dwarf galaxies ($L < 0.2 L_*$) are absent of the Mg II galaxy sample (Bergeron & Boissé 1991; Steidel 1993). At large redshift, several values of V_1 are considered although that chosen above is a good guess as it is similar to the dispersion of the C IV system velocity separation distribution (see Sect. 4).

The redshift z_i is determined by the assumption that $R_{\mathrm{lr}}(220\ \mathrm{km\,s^{-1}}, z_i) = R_{\mathrm{hr}}(220\ \mathrm{km\,s^{-1}}, z_i)$. Its exact value is of no importance as soon as $z_i > 1$. The other parameters are b_i, H_o, $R_{\mathrm{lr,o}}$ and f.

The derived variations of $\mathrm{d}N/\mathrm{d}z$ with z are compared in Fig. 11 to observations. Triangles are used for Mg II systems (Boissé et al. 1992; Steidel & Sargent 1992), squares for C IV systems (Steidel 1990a; Bahcall et al. 1993) and stars for Lyman limit systems (LLS) (Lanzetta 1991; Bahcall et al. 1993). The C IV sample for $z > 1$ is complete for $w_r(154.8) > 0.15$ Å whatever the doublet ratio in the C IV doublet is (Steidel 1990a). The low redshift measurement at $z = 0.3$ is that of the HST survey (Bahcall et al. 1993). It corresponds to systems with $w_r > 0.5$ Å and is thus a lower limit to the total number of C IV systems. We use the LLS survey by Lanzetta (1991) which gives the number of systems with optical depth at the Lyman limit $\tau > 1$. The number of such systems detected at $z \sim 0.65$ with the Hubble Space Telescope is significantly smaller. There are 5 LLS systems with $\tau > 1$ in the survey (see Table 8 of

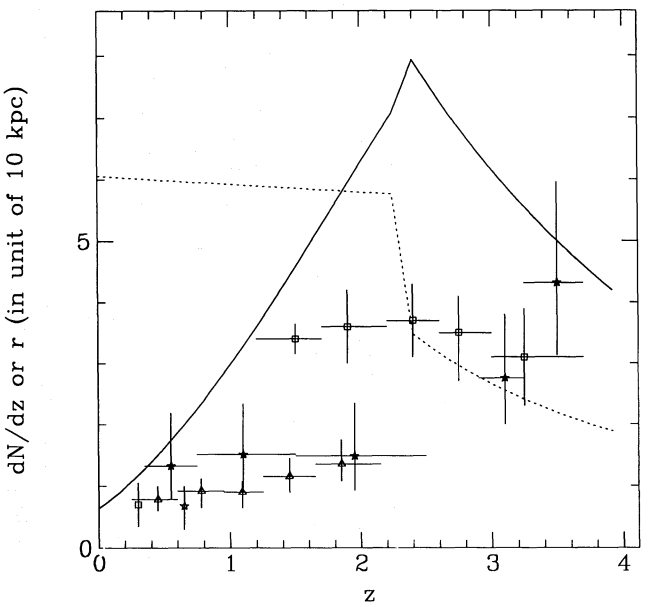

Fig. 11. Number of absorption systems per unit redshift (solid line) and radius of the haloes in units of 10 kpc (dashed line) versus redshift expected from CDM models (see Sect. 6). Overplotted are the observed numbers of C IV (squares), Mg II (triangles) and Lyman limit (stars) systems from Steidel (1990a), Steidel & Sargent (1992), Boissé et al. (1992) and Bahcall et al. (1993)

Bahcall et al. 1993). Even if we include the $z_{abs} = 0.474$ system in PKS1354 + 19 with $0.82 < \tau < 1.06$ and the $z_{abs} = 0.458$ Mg II system in 4C06.41 (Weymann et al. 1979) with $0.71 < \tau < 0.94$, we obtain using Eq. (7) of Bahcall et al. (1993) $dN(\tau > 1)/dz = 0.68$ at $z = 0.65$ which is nearly twice as small as the number given by Lanzetta (1991) $dN/dz = 1.3$. This indicates that the number of LLS from the IUE data may have been overestimated and that the number of LLS systems drop at low redshift. The sample of Mg II systems is complete for $w_r > 0.3$ Å. It has been shown that such Mg II absorption only arise in $\tau > 1$ systems (e.g. Bergeron & Stasińska 1986). This is consistent with the HST result for LLSs at $z \sim 0.4$–1.2. However if this result holds at lower redshift the number of Mg II systems at $z \sim 0.3$ derived by Boissé et al. (1992) $dN/dz = 0.66$ would indicate that the number of LLS systems does not drop dramatically for $z < 0.4$.

The curves in Fig. 11 correspond to $H_0 = 50\,\mathrm{km\,s^{-1}\,Mpc^{-1}}$, $V_l = 70\mathrm{km\,s^{-1}}$ and $b_i = 1.5$. From comparison of N-body simulation to large scale structures in the galaxy distribution, Davis et al. (1985) derive $b_i = 2.6$ but such a large value is inconsistent with the local galaxy velocity field (Lynden-Bell et al. 1988). We have adopted $R_{lr,0} = 70$ kpc which is the mean radius of a Mg II absorber (Bergeron & Boissé 1991; Steidel 1993) at low redshift and thus should be considered as a lower limit for C IV systems and $f = 1$. The dotted line corresponds to the mean radius of the absorber in units of 10 kpc.

It must be noticed that, for our model, the variations of dN/dz with z are quite independent of the chosen values of the parameters and are similar to those observed for C IV systems. At small redshift dN/dz increases because the number of haloes per unit volume increases with z and their radius depends only weakly on their circular velocity. At large redshift dN/dz decreases with z because r_0 is strongly decreasing.

The number of C IV systems at $z \sim 0.3$ is correctly reproduced by the model. For a value of H_0 as large as $100\,\mathrm{km\,s^{-1}\,Mpc^{-1}}$, dN/dz is too small at low z and b_i would then have to be larger than 2.5 to reproduce the HST point. This indicates that the above parameters are strongly constrained by the low redshift behavior of dN/dz. At large redshift, taking $H_0 = 100\,\mathrm{km\,s^{-1}\,Mpc^{-1}}$ implies that V_l must be smaller than $50\,\mathrm{km\,s^{-1}}$ in order to reproduce the number of LLS systems at $z > 3.5$. Such very low velocities are envisaged only for mini-haloes giving rise to metal-poor Lyα systems (Rees 1986).

At redshift $1.6 < z < 3.5$, the predicted number of systems is a factor of 1.5 too high as compared to the observed number of C IV systems. If V_l is given a value as small as $50\,\mathrm{km\,s^{-1}}$ which is the smallest value possible for these systems, $dN/dz = 10$ for $z = 2$ which is too large. This number could be reduced if the C IV absorption occurs only in the central part of the haloes which implies $f < 1$. It is however stricking to notice that taking $r = r_0/2$ gives dN/dz lower than the present observations. This implies that in order to explain the number of C IV systems C^{+3} must be present out to $r > r_0/2$ in all the haloes with $V_c > 50\,\mathrm{km\,s^{-1}}$ or out to $r \sim r_0$ in all the haloes with $V_c > 70\,\mathrm{km\,s^{-1}}$. This conclusion is strengthened by the fact that we did not take into account evolution of the abundances which would lower the number of systems at high redshift.

The observed number of LLS is steadily increasing with redshift and there is nothing in the observations indicating that this behavior might change at redshift larger than 3.6. In order to produce a number of systems per unit redshift larger than 5 at this redshift, a value of V_l smaller than $50\,\mathrm{km\,s^{-1}}$ is required. This indicates that there probably exists two populations of LLS at high redshift. Some would be associated with the metal systems and others with the Lyα clouds becoming optically thick at high redshift. In this case some evolution of the H I column density distribution with redshift is expected.

It can be seen from Fig. 11 that the evolution of Mg II systems is much flatter than predicted by the model indicating that Mg II and C IV systems seem to have different evolutions, which is not unexpected since Mg II systems arise mostly through the optically thick part of the haloes whereas C IV systems arise in the external highly ionized regions. Indeed the velocity structure of Mg II systems is known to evolve strongly with redshift (Caulet 1989; Petitjean & Bergeron 1990; Steidel & Sargent 1992).

Acknowledgements. We thank R.F. Carswell and J.K. Webb for providing us with a copy of their fitting program, P. Boissé for fruitful discussions and S. D'Odorico for making the CASPEC observations possible.

References

Aragón-Salamanca A., Ellis R.S., Schwartzenberg J.M., Bergeron J., 1993, MNRAS (in press)
Arnaud M., Rothenflug R., 1985, A&AS 60, 425
Atwood B., Baldwin J.A., Carswell R.F., 1985, ApJ 292, 58
Bahcall J.N, Bergeron J., Boksenberg A., Hartig G.F., Jannuzi B.T., Kirkhakos S., Sargent W.L.W., Savage B.D., Schneider D.P., Turnshek D., Weymann R.J., Wolfe A.M., 1993, ApJS (in press)
Bergeron J., 1986, A&AL 155, L8
Bergeron J., Boissé P., 1991, A&A 243, 344
Bergeron J., Stasińska, 1986, A&A 169, 1
Bergeron J., D'Odorico S., Kunth D., 1987, A&A 180, 1
Bergeron J., Cristiani S., Shaver P., 1992, A&A 257, 417
Blades J.C., 1988. in: Blades J.C., Turnshek D.A., Norman C.A. (eds.) QSO Absorbing lines: Probing the Universe. Cambridge University Press, Cambridge, p. 147
Boissé P., Bergeron J., 1985, A&A 145, 59
Boissé P., Boulade O., Kunth D., Tytler D., Vigroux L., 1992, A&A 262, 401
Boroson T., Sargent W.L.W., Boksenberg A., Carswell R.F., 1978, ApJ 220, 772
Carlberg R.G., Couchman H.M.P., 1989, ApJ 340, 47

Carswell R.F., Smith M.G., Whelan J.A.J., 1977, ApJ 216 351
Carswell R.F., Morton D.C., Smith M.G., Stockton A.N., Turnshek D.A., Weymann R.J., 1984, ApJ 278, 486
Carswell R.F., Lanzetta K.M., Parnell H.C., Webb J.K., 1991, ApJ 371, 36
Caulet A., 1989, ApJ 340, 90
Chen J.S., Morton D.C., 1984, MNRAS 208, 167
Colless M., Ellis R.S., Taylor K., Hook R.N., 1990, MNRAS 244, 408
Davis M., Efstathiou G., Frenk C., White S., 1985, ApJ 292, 371
de Boer K.S., Jura M.A., Shull J.M., 1987, in: Kondon Y., (ed.) The Scientific Accomplishments of the IUE. Reidel, Dordrecht, p. 485
Foltz C.B., Chaffee F.H. Jr., Black J.H., 1988, ApJ 324, 267
Foltz C.B., Hewett P.C., Chaffee F.H., Hogan C.J., 1993, AJ 105, 22
Frenk C.S., White S., Effstathiou G., Davis M., 1988, ApJ 327, 507
Giallongo E., Cristiani S., Fontana A., Trèvese D., 1993, ApJ (in press)
Kauffmann G., White S.D.M., 1993, MNRAS 261, 921
Lanzetta K.M., 1991, ApJ 375, 1
Lanzetta K.M., Bowen D.V., 1993, ApJ 391, 48
Lanzetta K.M., Turnshek D.A., Wolfe A.M., 1987, ApJ 322, 739
Levshakov S.A., Varshalovitch D.A., 1985, MNRAS 212, 517
Lyden-Bell D., Faber S.M., Burstein D., Davies R.L., Dressler A., Terlevich R.J., Wegner G., 1988, ApJ 326, 19
Meyer D.M., York D., 1987a, ApJ 315, L5
Meyer D.M., York D., 1987b, ApJ 319, L45
Meyer D.M., Welty D.E., York D.G., 1989, ApJ 343, L37
Mo H.J., Miralda-Escudé J., Rees M.J., 1993, MNRAS 264, 705
Møller P., Warren S.J., 1993, A&A (in press)
Morton D.C., 1991, ApJS 77, 119
Morton D.C., Chen J., Wright A.E., Peterson B.A., Jauncey D.L., 1980, MNRAS 193, 399
Morton D.C., York D.G., Jenkins E.B., 1988, ApJS 68, 449
Péquignot D., 1990, A&A 231, 499
Petitjean P., Bergeron J., 1990, A&A 231, 309
Petitjean P., Bergeron J., Puget J.L., 1992, A&A 265, 375
Petitjean P., Webb J.K., Rauch M., Carswell R.F., Lanzetta K., 1993, MNRAS 262, 499
Pettini M., Hunstead R.W., Murdoch H.S., Blades J.C., 1983, ApJ 273, 436
Press W.H., Schechter P., 1974, ApJ 187, 425
Rauch M., Carswell R.F., Chaffee F.H., Foltz C.B., Webb J.K., Weymann R.J., Bechtold J., Green R.F., 1992, ApJ 390, 387
Rees M.J., 1986, MNRAS 218, 25P
Sargent W.L.W., Young P.J., Boksenberg A., Carswell R.F., Whelan J.A.J., 1979, ApJ 230, 49
Sargent W.L.W., Young P.J., Boksenberg A., Tytler D., 1980, ApJS 42, 41
Sargent W.L.W., Boksenberg A., Steidel C.C., 1988, ApJS 68, 539
Sargent W.L.W., Steidel C.C., Boksenberg A., 1990, ApJ 351, 354
Savaglio S., D'Odorico S., Møller P., 1993, A&A (in press)
Sembach K.R., Savage B.D., 1992, ApJS 83, 147
Steidel C.C., 1990a, ApJS 72, 1
Steidel C.C., 1990b, ApJS 74, 37
Steidel C.C., 1993, in: Shull J.M., Thronson H. (eds.) The Evolution of Galaxies and Their Environment Proceeding of the Third Teton Summer Astrophysics Conference. Kluwer, Dordrecht (in press)
Steidel C.C., Sargent W.L.W., 1992, ApJS 80, 1
Wampler E.L., 1991, ApJ 368, 40
Wampler E.J., Bergeron J., Petitjean P., 1993, A&A 273, 15
Webb J.K., 1987, Ph.D. Thesis, Cambridge
Weymann R.J., Williams R.E., Peterson B.M., Turnshek D.A., 1979, ApJ 234, 33
Whelan J.A.J., Smith M.G., Carswell R.F., 1979, MNRAS 189, 363
White S.D.M., Frenk C.S., 1991, ApJ 379, 52
White S.D.M., Rees M.J., 1978, MNRAS 183, 341
Wolfe A., 1988, in: Blades J.C., Turnshek D.A., Norman C.A. (eds.) QSO Absorbing Lines: Probing the Universe. Cambridge University Press, Cambridge, p. 297
Wolfe A., 1986, in: Bregman J., Lockman J. (eds.) Proc. NRAO Conf. on Gaseous Halos of Galaxies. NRAO SP, p. 259
York D.G., Dopita M., Green R., Bechtold J., 1986, ApJ 311, 610
Young P., Sargent W.L.W., Boksenberg A., Carwell R.F., Whelan J.A.J., 1979, ApJ 229, 891
Young P., Sargent W.L.W., Boksenberg A., 1982, ApJS 48, 455